RSC Advances

PAPER

View Article Online
View Journal | View Issue

Cite this: *RSC Adv.*, 2017, **7**, 19694

Shape-controlled electrochemical synthesis of Au nanocrystals in reline: control conditions and electrocatalytic oxidation of ethylene glycol

Aoqi Li, Yujuan Chen, Wanyi Duan, Congyue Wang and Kelei Zhuo *

Gold nanocrystals (NCs) as advanced catalysts towards ethylene glycol (EG) electrooxidation in direct alcohol fuel cells (DAFCs) have some advantages, such as good poisoning-resistance and high electrocatalytic activity. The shape and size control of Au NCs are crucial to their electrocatalytic activity. In this work, the control of morphologies and sizes of prepared Au NCs in reline are systematically investigated by changing electrodeposition conditions: the applied potential, electrodeposition temperature, $HAuCl_4$ concentration and electrodeposition time. Results show that reline (a deep eutectic solvent (DES), a mixture of choline chloride and urea at the molar ratio of 1 : 2) plays an important part in the nucleation and growth of the star-like Au NCs. This approach for preparing star-like Au NCs in reline does not need any supporting electrolyte and organic solvent, and thus is more environmentally friendly than water as a medium. The electrode modified by the as-prepared Au nanostars (NSs) exhibits a good poisoning-resistance ability and electrocatalytic activity for EG electrooxidation in alkaline media. This strategy is a significant way for shape-controlled synthesis of noble metal nanomaterials in DESs that may have potential applications in fields of electrochemical sensors, electrocatalysis and fuel cells.

Received 9th February 2017
Accepted 28th March 2017

DOI: 10.1039/c7ra01639e

rsc.li/rsc-advances

Introduction

Nanocrystals (NCs) of gold and other noble metals have been widely used as promising catalysts for energy conversion and chemical transformations.[1,2] One of their important applications is to be used as catalysts in fuel cells due to their high electrocatalytic performance.[3,4] The electrooxidation of alcohols has come to be of significant interests because of its potential application in direct alcohol fuel cells (DAFCs) over the past few years.[5–7] To date, tremendous efforts have been made to investigate the electrooxidation of alcohols including methanol, ethanol, ethylene glycol (EG), propanol and glycerol.[8–11] Among alcohol fuels, methanol has been the most widely studied. Meanwhile, the other low molecular weight alcohols are also attractive alternative fuels for DAFCs on account of their lower toxicities and higher energy densities compared with methanol.[12] EG has higher energy density (7.56 kW h dm^{-3}) and boiling point (471 K) than other typical alcohol fuels such as methanol and ethanol.[13,14] And, surprisingly, EG can provide larger oxidation currents than methanol and polyols.[15] Consequently, EG is a more promising fuel for DAFCs than conventional direct methanol/ethanol fuel cells. Although Pt- and Pd-based NCs are the most active catalysts, Au NCs as advanced catalysts have additional advantages: good poisoning-resistance and low cost for EG electrooxidation in DAFCs.[16]

It is generally known that the catalytic performances of Au NCs depend strongly on their morphology, size, surface structure and crystallinity.[17–20] Therefore, the shape-controlled synthesis and relevant applications of Au NCs have been widely studied and obtained great success during the past decade. Many efforts have been devoted to the shape-controlled synthesis of Au NCs with different morphologies, such as nanospheres, nanorods, nanowires, nanodendrites, nanosheets, nanocombs and pentagon-shaped particles.[21–26] In general, Au NCs are prepared by using wet chemistry, hydrothermal synthesis, seeded growth and electrochemical synthesis.[27] Using chemical reduction methods, undesirable excessive reducing agents may increase the cost in mass production, contaminate the chemically reduced Au NCs, and affect the electrocatalytic performance. Alternatively, one-step electrodeposition, as a controllable, effective, convenient and environment-friendly method, has been developed for shape-controlled synthesis of Au NCs.[28,29]

Deep eutectic solvents (DESs) were first reported by Abbott and co-workers as a new generation of green solvents.[30] DESs can be usually produced by using quaternary ammonium salts mixed with hydrogen-bond donors such as amides, and thus are liquids at ambient temperature.[31] The properties of DESs are similar to those of ionic liquids, namely, high viscosity and conductivity, good thermal stability and negligible vapour

Collaborative Innovation Center of Henan Province for Green Manufacturing of Fine Chemicals, Key Laboratory of Green Chemical Media and Reactions, Ministry of Education, School of Chemistry and Chemical Engineering, Henan Normal University, Xinxiang, Henan 453007, P. R. China. E-mail: klzhuo@263.net; Fax: +86-373-3329056; Tel: +86-373-3329056

pressure. Moreover, DESs have additional advantages: non-toxicity, biodegradation, low cost and environment-friendliness.[32,33] Because of their remarkable physicochemical properties, DESs as promising solvents have broad applications in electrochemistry, metal–organic frameworks and catalysis.[34–36] In recent years, the synthesis of nanomaterials in DESs has received a lot of attention.[37–42] However, to the best of our knowledge, there are yet very few reports of the use of DESs in the shape-controlled synthesis of Au NCs by using electrodeposition method.

In our previous work, Au NCs with different morphologies were successfully prepared in three DESs with different contents of water.[28] It is worth noting that the water content was used as a key factor to control the morphology and structure of Au NCs. Herein, we carried out a systematic research on shape-controlled synthesis of Au NCs in reline (a DES) by controlling different electrodeposition conditions, such as the applied potential, electrodeposition temperature, $HAuCl_4$ concentration and electrodeposition time. In the preparation of Au nanostars (NSs), reline acted as not only solvent but also shape-directing agent for the formation and growth of the star-like nanostructures. Compared with water system, this approach for the preparation of Au NSs in reline is more environment-friendly. Furthermore, the electrocatalytic performance of the Au NSs was studied, showing a good poisoning-resistant ability and high electrocatalytic activity for EG electrooxidation in alkaline media.

Experimental

Chemicals

Choline chloride ($HOC_2H_4N(CH_3)_3Cl$, 98%), urea (NH_2CONH_2, 99.5%) and ethylene glycol (99.0%) were purchased from Sigma-Aldrich Co. LLC. Tetrachloroauric(III) acid tetrahydrate ($HAuCl_4 \cdot 4H_2O$) was purchased from Sinopharm Chemical Reagent Co., Ltd and used without further purification. All aqueous solutions were prepared with twice-distilled water.

Preparation of DES

Choline chloride (ChCl) was recrystallized from absolute ethanol, filtered and dried under vacuum. Urea (U) was dried under vacuum before use. A DES was formed by stirring ChCl and U (reline, molar ratio: (ChCl)/U = 1/2) at 80 °C until homogeneous and colourless liquids.[3,28,31] The prepared reline, once formulated, was kept in a vacuum at 80 °C prior to use.

Synthesis of Au NSs in reline

The electrochemical synthesis of Au NCs in reline was carried out by using a standard three-electrode cell connected to a CHI 660D electrochemical workstation (Shanghai Chenhua Instrumental Co., Ltd., China), with a Pt wire counter electrode, a Pt quasi-reference electrode, and a glassy carbon electrode (GCE, 3 mm in diameter) as the working electrode. The GCE was polished, in turn, with 1.0, 0.3, and 0.05 μm Al_2O_3 powder and rinsed thoroughly with twice-distilled water. Then, the electrode was subsequently washed in ethanol and twice-distilled water by ultrasonication and dried by nitrogen before each experiment.[21,37] In a typical procedure as described in our previous work,[28] Au NSs with sharply pointed structures were electrodeposited directly on a GCE under the applied potential of −0.60 V (*vs.* Pt) in 20 mM $HAuCl_4$ reline solution at 90 °C for 600 s.

Characterization

The size and morphology of prepared Au NCs were characterized by field emission scanning electron microscopy (FESEM, ZEISS SUPRA 40) and transmission electron microscopy (TEM, JEOL JEM 2100). The X-ray photoelectron spectroscopy (XPS) measurements were conducted using a Thermo Scientific ESCALAB 250Xi with the Al Kα X-ray source (1486.6 eV).

Electrocatalytic performance measurements

The electrocatalytic performances of the Au NSs towards EG oxidation were evaluated by cyclic voltammetry (CV) in 0.5 M NaOH solution at room temperature. A saturated calomel electrode (SCE) was used as reference electrode, and all potentials in the electrochemical performance tests were quoted *versus* the SCE scale.

Results and discussion

Effects of electrodeposition conditions

Firstly, we devote ourselves to systematically investigating effects of different electrodeposition conditions on morphologies and sizes of prepared Au NCs by the potentiostatic electrodeposition method as described in our previous work.[28] One-step electrodeposition is a powerful and effective method for shape-controlled synthesis of Au NCs. The applied potential plays a vital role for the nucleation and growth of Au NCs in the process of electrodeposition. Au NCs with different morphologies and sizes were prepared at different applied potentials ranging from −0.40 to −1.60 V (*vs.* Pt) in reline containing 20 mM $HAuCl_4$ for 600 s. As shown in Fig. 1a, when the applied potential is −0.50 V, a large number of irregular nanoparticles and a few of Au NCs with tips and thorns were obtained. Using the potential of −0.60 V (Fig. 1b), Au NCs with unique star-like and sharply pointed nanostructures were synthesized on the GCE. When the applied potential negatively moved to −0.70 V (Fig. 1c), lots of Au NCs with rod-like structures were produced instead of tips and thorns. Apparently, Au NSs with well-crystallized and uniform star-like nanostructures could be synthesized in reline only at −0.60 V. The reason for the morphology control of Au NCs by the applied potential is that the applied potential determines the current and the reaction rate, and thus affects the eventual morphologies and structures of Au deposits. Meanwhile, *I–t* curves of prepared Au NCs under electrodeposition potentials of −0.50, −0.60 and −0.70 V are shown in Fig. 1d. It can be seen from curves a and c that a large reduction current appears first, then decreases to a low value rapidly, and finally reaches a stable value as time progresses. However, at the electrodeposition potential of −0.60 V (Fig. 1d, curve b), a large reduction current decreases rapidly to a lowest value (hump), then increases gradually, and finally trends to

a stable value. The appearance of the hump (curve b) may be ascribed to the electrochemical nucleation and growth of Au NSs with the star-like morphology and specific structure at this particular applied potential.[43]

It is worthwhile noting that the electrodeposition temperature is also a key factor to control morphologies and sizes of nanocrystals. Fig. 2 shows the FESEM images of Au NCs obtained at different electrodeposition temperatures. At lower electrodeposition temperatures, such as 70 and 80 °C (Fig. 2a and b), some small irregular quasi-spherical nanoparticles with few thorns were prepared. However, at higher electrodeposition temperatures, such as 100 and 110 °C (Fig. 2c and d), the star-like nanostructures became irregular and their sizes increased owing to the overgrowth of sharply pointed structures and thorns. These can be explained as follows. At low temperatures, the energy state of reaction system is relatively low, the nucleation and growth of NCs into the thermodynamically favored equilibrium morphologies are preferred under a thermodynamically controlled regime, hence nanoparticles grow into quasi-spherical nanostructures.[44] When the temperature of reaction reaches a certain level, such as 90 °C, the nucleation and growth of NCs are facilitated under a kinetically controlled regime. Meanwhile, reline as a special shape-directing agent plays a key role in shape control for the nucleation and growth of NCs at high temperature, leads to an orienting growth of NCs. When the temperature gets too high, the obtained NCs overgrow. Therefore, such an obvious difference in size and morphology of Au NCs prepared at different temperatures are owing to the variation of reaction environments with the temperature, which causes the diffusion of reactive species in reline and thus influences the nucleation and growth process of Au NCs on GCE.[30]

The morphologies and sizes of Au deposits are also sensitive to the concentrations of $HAuCl_4$ in reline. Fig. 3 shows the FESEM images of Au NCs prepared in different concentrations

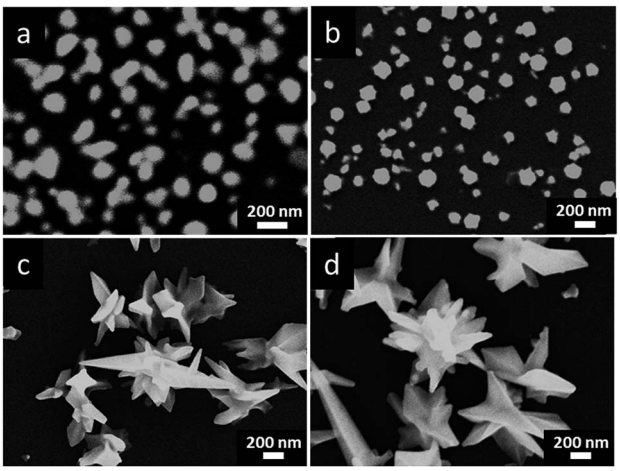

Fig. 2 FESEM images of prepared Au NCs under the applied potential of −0.60 V (*vs.* Pt) in 20 mM $HAuCl_4$ reline solution for 600 s at different electrodeposition temperatures: (a) 70 °C, (b) 80 °C, (c) 100 °C and (d) 110 °C.

of $HAuCl_4$. In 2 mM $HAuCl_4$ (Fig. 3a), newly generated Au clusters covered on the GCE, leading to anisotropic growth of many small and immature nanocrystals. In 5 mM $HAuCl_4$ (Fig. 3b), a few of Au NCs with tips and thorns were formed, while most of Au NCs were irregular nanocrystals. When the $HAuCl_4$ concentrations increased to 10 mM (Fig. 3c), there were a large number of Au NCs with sharply pointed structures and thorns appeared on the GCE, accompanied with a few immature star-like nanostructures. In the $HAuCl_4$ concentration of 20 mM, the Au NSs with well-crystallized and unique star-like nanostructures were homogeneously synthesized (see Fig. 1b). Further increasing $HAuCl_4$ concentrations to 30 mM (Fig. 3d), the structure of prepared Au NCs became complex and irregular, and their sizes increased. The concentration dependence of the Au nanostructures maybe result from the high viscosity of reline, which decreased the mass transportation of reactive

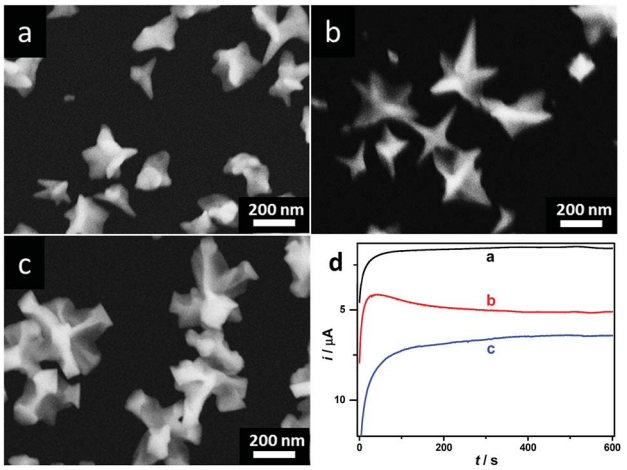

Fig. 1 FESEM images of the Au NCs obtained in 20 mM $HAuCl_4$ reline solution at 90 °C for 600 s under different applied potentials: (a) −0.50 V, (b) −0.60 V and (c) −0.70 V (*vs.* Pt). (d) Current–time curves for preparation of the Au NCs: curves a, b and c are corresponding to (a)–(c), respectively.

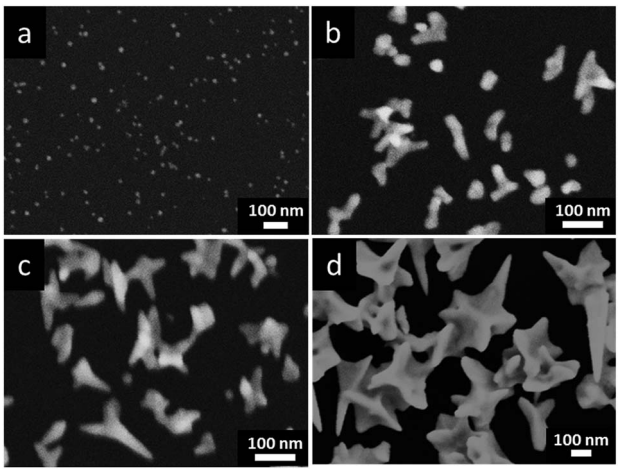

Fig. 3 FESEM images of prepared Au NCs under the applied potential of −0.60 V (*vs.* Pt) at 90 °C for 600 s in different concentrations of $HAuCl_4$ in reline: (a) 2 mM, (b) 5 mM, (c) 10 mM and (d) 30 mM.

species in reline, and consequently it is difficult to form Au NSs with sharply pointed structures in low $HAuCl_4$ concentrations.[31]

Among all conditions, the electrodeposition time reflects the morphological evolution of Au NSs growth. Au NCs with different morphologies generated through different electrodeposition time are shown in Fig. 4. After electrodeposition of 100 s (Fig. 4a), many small irregular nanothorns and tiny Au nanoparticles of ~100 nm appeared, which acted as precursors for subsequently producing Au NSs. Since the nucleation process is instantaneous and irreversible, newly generated Au atoms favour growing on the original Au nuclei instead of generating more new nuclei.[45] When the deposition continues for 300 s (Fig. 4b), the star-like nanostructures began to show, but nanocrystals had not grown fully. After 600 s, the well-defined Au NSs were emerged (Fig. 1b). Increasing the electrodeposition time to 900 s, a lot of complex irregular monodisperse nanostars with more sharply pointed and larger size were detected (Fig. 4c). Further prolonging the electrodeposition time to 1200 s, the Au NSs were over-growing and became very big and irregular (Fig. 4d). Therefore, nucleation and adsorption are clearly fast stages, while the morphology adjustment and subsequent pointed growth are a slow process controlled by kinetic model, which is regarded as the predominant factor.[46]

To sum up, the morphologies and sizes of Au NCs could be controlled jointly by these electrodeposition conditions: the applied potential, electrodeposition temperature, $HAuCl_4$ concentration and electrodeposition time.

To carefully characterize morphologies and sizes of the prepared Au NSs, FESEM and TEM experiments were carried out. The FESEM images of the typical Au NSs were shown in Fig. 5a and b. It can be seen that lots of Au NSs with sharply pointed structures and thorns were homogeneously formed on the GCE. Furthermore, high-magnification FESEM and TEM images (Fig. 5c and d) reveal the details of the Au NSs. The crystal orientation and composition of Au NSs were further

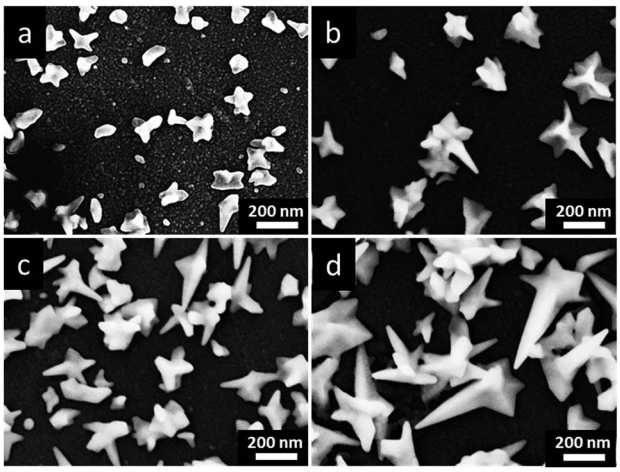

Fig. 4 FESEM images of prepared Au NCs under the applied potential of −0.60 V (*vs.* Pt) in 20 mM $HAuCl_4$ reline solution at 90 °C for different electrodeposition time: (a) 100 s, (b) 300 s, (c) 900 s and (d) 1200 s.

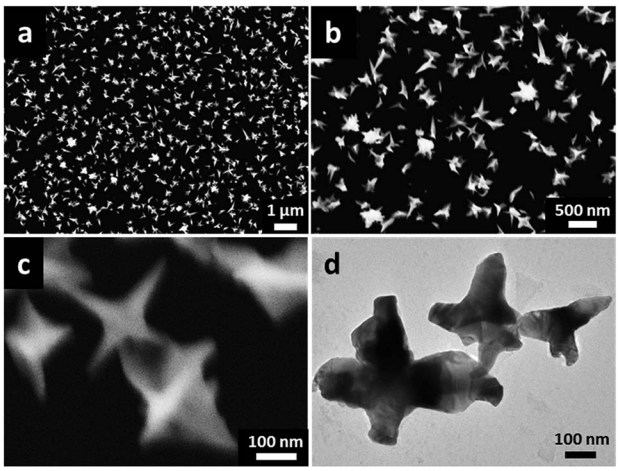

Fig. 5 (a) and (b) Low-magnification FESEM, (c) high-magnification FESEM, (d) TEM images of prepared Au NSs on GCE under the applied potential of −0.60 V (*vs.* Pt) in 20 mM $HAuCl_4$ reline solution at 90 °C for 600 s.

investigated by high resolution TEM (HRTEM) and XPS. Fig. 6a shows a single star-like Au NC, which enables an examination of its growth direction. As seen in Fig. 6b, a spinous tip of the nanostar structure shows clear lattice fringes with the same orientation and *d*-spacing. The *d* value of 0.24 nm is corresponding to the (111) lattice spacing of the face-centered cubic (fcc) Au crystals, consistent with other Au nanostructures reported in the literature.[47] This reveals that the growth of the Au NSs preferentially occurs along the ⟨111⟩ direction. The XPS pattern of the Au NSs (Fig. 6b) exhibits two significant Au 4f peaks at the binding energy of 83.98 eV (Au $4f_{7/2}$) and 87.68 eV (Au $4f_{5/2}$), which are assigned to metallic Au.[48] Thus, the result confirms that as-prepared nanostructure is composed of metallic Au.

Formation mechanism of the Au NSs

The final morphologies and sizes of metallic NCs can be significantly influenced by the growth kinetics of the crystal nuclei. The main criterion proposed to achieve kinetic control is that the reaction should proceed considerably slower than under normal conditions.[46] In our work, the anisotropic growth of Au NCs into a star-like morphology in reline by substantially slowing down the reaction which deviates from the equilibrium

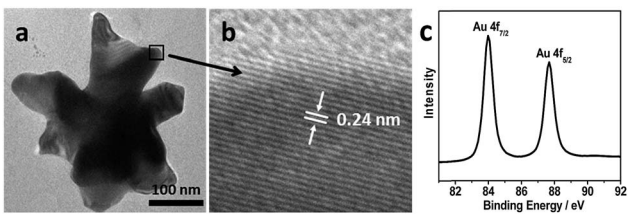

Fig. 6 (a) TEM image of the Au NSs and (b) HRTEM image of the spinous tip of the Au NS marked in (a). (c) XPS spectrum of prepared Au NSs.

morphology is facilitated under kinetic control. Similar observations were obtained by constructing anisotropic nanostructures (Au nanoflowers) in DES.[37]

A three-staged formation mechanism is proposed to elucidate the formation process of the Au NSs in reline: (1) nucleation, (2) evolution of nuclei into seeds and (3) growth of seeds into nanocrystals. Firstly, at the very early stage, a large amount of Au^{3+} ions were instantaneously reduced to Au atoms, and the reduced Au atoms aggregated together to form Au nuclei, and randomly distributed on the GCE surface, *i.e.*, instantaneous nucleation process.[49] Secondly, the adjacent urea molecules in reline were rapidly and selectively adsorbed on the specific Au crystal planes to formed a monolayer by self-assembly, which would prevent newly generated Au atoms to further aggregate. Moreover, two $-NH_2$ groups of each urea molecule in reline were likely to break the equilibrium of reaction and produce star-like and sharply pointed nanostructures, resulting into the Au ⟨111⟩ direction growth (see the HRTEM characterization, Fig. 6b).[46,50] This might be due to selective adsorption, the interactions between Au and $-NH_2$ groups (Au–NH_2), and steric hindrance of reline.[24] Therefore, the newly emerged Au atoms preferentially aggregated on initial Au nuclei instead of other GCE surface, and subsequently develop to seeds with specific structures. Thirdly, since urea molecules, acting as shape-directing agents interact with the seeds, the growth of Au NSs occurred at the initial tips and thorns, and finally the seeds grew into the star-like NCs, which is a slow process dominated by the kinetic control.[18,22]

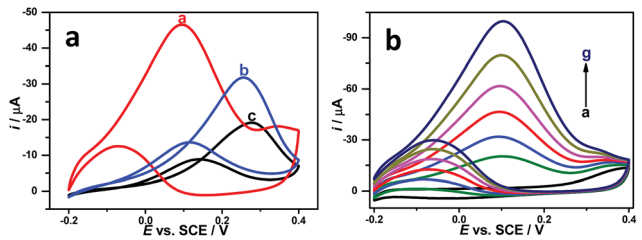

Fig. 7 (a) CVs of the GCE modified with Au NSs (curve a) and irregular Au NCs (curve b) and commercial Au electrode (curve c) in 0.5 M NaOH solution containing 0.10 M EG with a scan rate of 50 mV s^{-1}. (b) The catalytic responses of the Au NSs modified electrode in 0.5 M NaOH and different concentrations of EG (curve a–g): 0, 0.04, 0.07, 0.10, 0.13, 0.16 and 0.19 M with a scan rate of 50 mV s^{-1}.

In addition, in other DESs (ethaline and glyceline) containing –OH groups instead of $-NH_2$ groups, morphologies of Au NCs prepared in similar conditions are different from Au NSs.[28] This confirms further that the $-NH_2$ groups of urea in reline could control the formation and oriented growth of star-like Au NCs. To sum up, in the formation process of Au NSs, reline acted as not only solvent but also shape-directing agent. In addition, this approach for preparing Au NSs in reline does not need any supporting electrolyte such as sulfuric acid and organic solvent, and thus is more environment-friendly than water as medium.

Electrocatalytic performance of the Au NSs

As is well-known, gold nanomaterials exhibit a good electrocatalytic activity towards EG oxidation, which depends strongly on their sizes and morphologies.[51] The electrocatalytic activities of the Au NSs (with sharply pointed structures at the applied potential of −0.60 V, *vs.* Pt), the irregular Au NCs (with rod-like structures at the applied potential of −0.70 V, *vs.* Pt) and commercial Au electrode towards EG oxidation were evaluated by CV in 0.5 M NaOH solution containing 0.10 M EG (Fig. 7a). As shown in Fig. 7a, the prepared Au NSs exhibit higher electrocatalytic current than the irregular Au NCs and commercial Au electrode. Moreover, the peek potential of Au NSs modified electrode is 0.10 V (*vs.* SCE, Fig. 7a, curve a), which is more negative than the irregular Au NCs modified electrode with a value of 0.26 V (Fig. 7a, curve b) and commercial Au electrode with a value of 0.28 V (Fig. 7a, curve c). These phenomena reveal more catalytic active sites and larger electroactive surface area of the Au NSs, which are attributed to the specific structure and star-like morphology of prepared Au NSs.

In addition, a cathodic peak of the electrode modified by as-prepared Au NSs appears at −0.07 V in the reverse scan, corresponding to the electrochemical oxidation of CO, acetaldehyde, and CH_x poisoning intermediates.[48,51] Larger ratio of the peak currents in the forward potential scan (i_f) to the reverse scan (i_r) would bring better poisoning-resistant ability of the electrodes for EG oxidation. The oxidation peak in the backward scan corresponds to the electrochemical oxidation of CO and other adsorbed species. The value of i_f/i_r for the Au NSs is 3.71 (Fig. 7a). Moreover, this value is much higher than the irregular Au NCs (2.33), commercial Au electrode (2.16) and previously reported catalysts (Table 1),[7,51–56] showing that the Au NSs have better

Table 1 Comparative electrocatalytic performances of different catalysts towards EG oxidation in alkaline media in terms of forward peak current density (j_p) and ratio of forward to reverse peak current (i_f/i_r)

Electrocatalyst	Alcohol solution	j_p	i_f/i_r	Ref.
Au NSs	0.1 M EG/0.5 M NaOH	26.0 (mA mg^{-1})	3.71	This work
FeCo@Fe@Pd/C	0.5 M EG/0.5 M KOH	5.01 (mA cm^{-2})	2.64	7
Au NDs	0.7 M EG/0.5 M NaOH	4.96 (mA cm^{-2})	2.17	51
AuNPs/PG	0.6 M EG/0.1 M NaOH	25.0 (mA cm^{-2})	2.27	52
Pt–Pd multipods	1.0 M EG/1.0 M KOH	72.0 (mA cm^{-2})	3.64	53
S-MWNTs/Pd	0.5 M EG/0.2 M KOH	177.2 (mA mg^{-1})	1.94	54
SF-MWCNT–$PdSn_{mix}$	0.5 M EG/0.5 M KOH	51.9 (mA cm^{-2})	2.10	55
hAg@Pt–RGO	0.75 M EG/1.0 M KOH	120.3 (mA cm^{-2})	1.72	56

poisoning-resistant ability and steady-state behaviour for EG oxidation. Fig. 7b shows the typical CVs of the Au NSs modified electrode by successive addition of EG into 0.5 M NaOH solution. After injection of EG into the solution, the electrode responded quickly to reach the maximum current. Meanwhile, the corresponding catalytic currents increased linearly. The results indicated that as-prepared Au NSs have good poisoning-resistant ability and high electrocatalytic activity for EG oxidation.

Conclusions

In summary, the morphologies and sizes of Au NCs in reline could be tuned jointly by controlling different electrodeposition conditions, such as the applied potential, electrodeposition temperature, $HAuCl_4$ concentration and electrodeposition time. In the preparation process of Au NSs, any additive, template, surfactant and seed were not needed, indicating that reline acted as not only solvent but also shape-directing agent. Obviously, this method for the preparation of Au NSs in reline is more environment-friendly compared with water as medium. Furthermore, the Au NSs exhibited a better poisoning-resistant ability and higher electrocatalytic activity for EG oxidation in alkaline media than irregular Au NCs. We believe that this strategy would have significant implications for shape-controlled synthesis of noble metal nanomaterials in DESs, and provides great potentials for electrocatalysis and fuel cells.

Acknowledgements

Financial support from the National Natural Science Foundation of China (No. 21173070, 21303044, 21573058), Program for Innovative Research Team in Science and Technology in University of Henan Province (15IRTSTHN 003, 17IRTSTHN 001) are gratefully acknowledged.

Notes and references

1 H. L. Liu, F. Nosheen and X. Wang, *Chem. Soc. Rev.*, 2015, **44**, 3056–3078.
2 K. I. Ozoemena, *RSC Adv.*, 2016, **6**, 89523–89550.
3 L. Wei, Z. Y. Zhou, S. P. Chen, C. D. Xu, D. Su, M. E. Schuster and S. G. Sun, *Chem. Commun.*, 2013, **49**, 11152–11154.
4 H. Mao, T. Huang and A. Yu, *J. Alloys Compd.*, 2016, **676**, 390–396.
5 X. Zhang, Z. Tian and P. K. Shen, *Electrochem. Commun.*, 2013, **28**, 9–12.
6 L. Z. Li, M. X. Chen, G. B. Huang, N. Yang, L. Zhang, H. Wang, Y. Liu, W. Wang and J. P. Gao, *J. Power Sources*, 2014, **263**, 13–21.
7 O. O. Fashedemi and K. I. Ozoemena, *Electrochim. Acta*, 2014, **128**, 279–286.
8 Z. Y. Bai, M. Shi, Y. X. Zhang, Q. Zhang, L. Yang, Z. X. Yang and J. J. Zhang, *Green Chem.*, 2016, **18**, 386–391.
9 M. B. Rohwer, R. M. Modibedi and K. I. Ozoemena, *Electroanalysis*, 2015, **27**, 957–963.
10 J. N. Tiwari, R. N. Tiwari, G. Singh and K. S. Kim, *Nano Energy*, 2013, **2**, 553–578.
11 P. M. Ejikeme, K. Makgopa, K. Raju and K. I. Ozoemena, *ChemElectroChem*, 2016, **3**, 2243–2251.
12 F. Kosaka, Y. Oshima and J. Otomo, *Electrochim. Acta*, 2011, **56**, 10093–10100.
13 H. Yue, Y. Zhao, X. Ma and J. Gong, *Chem. Soc. Rev.*, 2012, **41**, 4218–4244.
14 O. O. Fashedemi, H. A. Miller, A. Marchionni, F. Vizza and K. I. Ozoemena, *J. Mater. Chem. A*, 2015, **3**, 7145–7156.
15 L. Xin, Z. Y. Zhang, J. Qi, D. Chadderdon and W. Z. Li, *Appl. Catal., B*, 2012, **125**, 85–94.
16 C. A. Angelucci, H. Varela, G. Tremiliosi-Filho and J. F. Gomes, *Electrochem. Commun.*, 2013, **33**, 10–13.
17 Y. Xia, X. Xia and H. C. Peng, *J. Am. Chem. Soc.*, 2015, **137**, 7947–7966.
18 H. Zhang, M. Jin and Y. Xia, *Angew. Chem., Int. Ed.*, 2012, **51**, 7656–7673.
19 X. Wang, S. I. Choi, L. T. Roling, M. Luo, C. Ma, L. Zhang, M. Chi, J. Liu, Z. Xie, J. A. Herron, M. Mavrikakis and Y. Xia, *Nat. Commun.*, 2015, **6**, 7594–7601.
20 P. C. Pandey, S. Shukla and Y. Pandey, *RSC Adv.*, 2016, **6**, 80549–80556.
21 J. J. Feng, A. Q. Li, Z. Lei and A. J. Wang, *ACS Appl. Mater. Interfaces*, 2012, **4**, 2570–2576.
22 J. J. Feng, Z. Y. Lv, S. F. Qin, A. Q. Li, Y. Fei and A. J. Wang, *Electrochim. Acta*, 2013, **102**, 312–318.
23 H. C. Peng, J. Park, L. Zhang and Y. Xia, *J. Am. Chem. Soc.*, 2015, **137**, 6643–6652.
24 Z. Y. Lv, A. Q. Li, Y. Fei, Z. Li, J. R. Chen, A. J. Wang and J. J. Feng, *Electrochim. Acta*, 2013, **109**, 136–144.
25 C. Zhu, H. C. Peng, J. Zeng, J. Liu, Z. Gu and Y. Xia, *J. Am. Chem. Soc.*, 2012, **134**, 20234–20237.
26 M. Tohidi, F. A. Mahyari and A. Safavi, *RSC Adv.*, 2015, **5**, 32744–32754.
27 Y. Xia, Y. Xiong, B. Lim and S. E. Skrabalak, *Angew. Chem., Int. Ed.*, 2009, **48**, 60–103.
28 A. Li, Y. Chen, K. Zhuo, C. Wang, C. Wang and J. Wang, *RSC Adv.*, 2016, **6**, 8786–8790.
29 J. Ping, Y. Wang, K. Fan, J. Wu and Y. Ying, *Biosens. Bioelectron.*, 2011, **28**, 204–209.
30 A. P. Abbott, G. Capper, D. L. Davies, R. K. Rasheed and V. Tambyrajah, *Chem. Commun.*, 2003, **23**, 70–71.
31 A. P. Abbott, D. Boothby, G. Capper, D. L. Davies and R. K. Rasheed, *J. Am. Chem. Soc.*, 2004, **126**, 9142–9147.
32 A. Paiva, R. Craveiro, I. Aroso, M. Martins, R. L. Reis and A. R. C. Duarte, *ACS Sustainable Chem. Eng.*, 2014, **2**, 1063–1071.
33 A. P. Abbott, R. C. Harris, F. Holyoak, G. Frisch, J. Hartley and G. R. T. Jenkin, *Green Chem.*, 2015, **17**, 2172–2179.
34 D. V. Wagle, H. Zhao and G. A. Baker, *Acc. Chem. Res.*, 2014, **47**, 2299–2308.
35 V. S. Raghuwanshi, M. Ochmann, F. Polzer, A. Hoell and K. Rademann, *Chem. Commun.*, 2014, **50**, 8693–8696.
36 Q. Q. Xiong, J. P. Tu, X. Ge, X. L. Wang and C. D. Gu, *J. Power Sources*, 2015, **274**, 1–7.
37 L. Wei, Y. J. Fan, H. H. Wang, N. Tian, Z. Y. Zhou and S. G. Sun, *Electrochim. Acta*, 2012, **76**, 468–474.

38 L. Wei, Y. J. Fan, N. Tian, Z. Y. Zhou, X. Q. Zhao, B. W. Mao and S. G. Sun, *J. Phys. Chem. C*, 2012, **116**, 2040–2044.
39 H. G. Liao, Y. X. Jiang, Z. Y. Zhou, S. P. Chen and S. G. Sun, *Angew. Chem., Int. Ed.*, 2008, **47**, 9100–9103.
40 C. Gu and J. Tu, *Langmuir*, 2011, **27**, 10132–10140.
41 X. Ge, C. D. Gu, Y. Lu, X. L. Wang and J. P. Tu, *J. Mater. Chem. A*, 2013, **1**, 13454–13461.
42 C. D. Gu, H. Zheng, X. L. Wang and J. P. Tu, *RSC Adv.*, 2015, **5**, 9143–9153.
43 J. J. Feng, A. Q. Li, A. J. Wang, Z. Lei and J. R. Chen, *Microchim. Acta*, 2011, **173**, 383–389.
44 B. Viswanath, P. Kundu, A. Halder and N. Ravishankar, *J. Phys. Chem. C*, 2009, **113**, 16866–16883.
45 T. M. Day, P. R. Unwin, N. R. Wilson and J. V. Macpherson, *J. Am. Chem. Soc.*, 2005, **127**, 10639–10647.
46 J. Xiao and L. Qi, *Nanoscale*, 2011, **3**, 1383–1396.
47 T. H. Lin, C. W. Lin, H. H. Liu, J. T. Sheu and W. H. Hung, *Chem. Commun.*, 2011, **47**, 2044–2046.
48 D. J. Chen, Q. L. Zhang, J. X. Feng, K. J. Ju, A. J. Wang, J. Wei and J. J. Feng, *J. Power Sources*, 2015, **287**, 363–369.
49 B. Scharifker and G. Hills, *Electrochim. Acta*, 1983, **28**, 879–889.
50 Y. Qin, Y. Song, T. Huang and L. Qi, *Chem. Commun.*, 2011, **47**, 2985–2987.
51 Y. F. Li, J. J. Lv, A. J. Wang, M. Zhang, R. Z. Wang and J. J. Feng, *J. Solid State Electrochem.*, 2015, **19**, 3185–3193.
52 M. Etesami and N. Mohamed, *Sci. China: Chem.*, 2011, **55**, 247–255.
53 J. J. Lv, L. P. Mei, X. Weng, A. J. Wang, L. L. Chen, X. F. Liu and J. J. Feng, *Nanoscale*, 2015, **7**, 5699–5705.
54 Z. P. Sun, X. G. Zhang, Y. Y. Liang and H. L. Li, *J. Power Sources*, 2009, **191**, 366–370.
55 T. Ramulifho, K. I. Ozoemena, R. M. Modibedi, C. J. Jafta and M. K. Mathe, *J. Electroanal. Chem.*, 2013, **692**, 26–30.
56 J. N. Zheng, J. J. Lv, S. S. Li, M. W. Xue, A. J. Wang and J. J. Feng, *J. Mater. Chem. A*, 2014, **2**, 3445–3451.